Solid-liquid coexistence in small systems: A statistical method to calculate melting temperatures

Qi-Jun Hong and Axel van de Walle

Citation: The Journal of Chemical Physics **139**, 094114 (2013); doi: 10.1063/1.4819792
View online: http://dx.doi.org/10.1063/1.4819792
View Table of Contents: http://scitation.aip.org/content/aip/journal/jcp/139/9?ver=pdfcov
Published by the AIP Publishing

Solid-liquid coexistence in small systems: A statistical method to calculate melting temperatures

Qi-Jun Hong[1,2,a] and Axel van de Walle[2,3]
[1]*Division of Chemistry and Chemical Engineering, California Institute of Technology, Pasadena, California 91125, USA*
[2]*School of Engineering, Brown University, Providence, Rhode Island 02912, USA*
[3]*Department of Applied Physics and Materials Science, California Institute of Technology, Pasadena, California 91125, USA*

(Received 23 April 2013; accepted 16 August 2013; published online 5 September 2013)

We propose an efficient and accurate scheme to calculate the melting point (MP) of materials. This method is based on the statistical analysis of small-size coexistence molecular dynamics simulations. It eliminates the risk of metastable superheated solid in the fast-heating method, while also significantly reducing the computer cost relative to the traditional large-scale coexistence method. Using empirical potentials, we validate the method and systematically study the finite-size effect on the calculated MPs. The method converges to the exact result in the limit of large system size. An accuracy within 100 K in MP is usually achieved when simulation contains more than 100 atoms. Density functional theory examples of tantalum, high-pressure sodium, and ionic material NaCl are shown to demonstrate the accuracy and flexibility of the method in its practical applications. The method serves as a promising approach for large-scale automated material screening in which the MP is a design criterion. © *2013 AIP Publishing LLC*. [http://dx.doi.org/10.1063/1.4819792]

I. INTRODUCTION

Theoretical predictions of the melting point (MP) have a long history, and have been based on a wide variety of calculation approaches, as well as different levels of accuracy in the descriptions of interatomic interactions. In the last two decades, thanks to the increased availability of computing power, density functional theory (DFT)[1–3] has established itself as a useful simulation tool for accurate and general modeling of materials, but melting point predictions based on DFT are still considered quite challenging, involving either the use of large simulation cells or the development of auxiliary empirical potentials. In this paper, we seek to relax the requirements by exploring the possibility of accurately and quickly predicting MP using small-cell DFT calculations alone. Such a capability would be very useful, for instance, in the study of phase diagrams of novel materials or in the automated screening of materials when MP enters in the selection criterion.

Our primary goal is to devise a method that delivers a melting point estimate simply and quickly, and whose accuracy can be systematically improved if more calculations are performed. This capability is ideal for material screening efforts, but, unfortunately, current methods commonly used in MP calculations do not have this property. For example, free energy-based methods,[4–9] in which MP is located at the intersection of free energy curves, suffer from the high computational cost of liquid-state free energy calculations and/or the reliance on reference systems with known free energy, which may be difficult to devise in complex materials. Another mainstream method, the solid-liquid coexistence approach,[10–14] requires a large system size to stabilize the coexistence, thus rendering the method computationally demanding in the context of DFT. In each case, the methods have a large "fixed cost," both in terms of computational and human effort, that is hard to reduce even if a lower accuracy is sufficient. The fast-heating method, or so-called "heat-until-it-melts" method,[15] has lower computational requirements but exhibits hysteresis and overheating issues near phase transition. The "Z-method,"[16] although successfully applied to several systems,[17,18] is still under debate[17,19,20] on its rigorous theoretical ground and its heavy dependence on simulation size and length.

Despite of their disadvantages, both the coexistence and the fast-heating methods shed light on the search of an automated MP predictor, as they are complementary to each other. For example, while the coexistence method demands large system size, which skyrockets the computer cost, the fast-heating method requires only a small size. Also, while the fast-heating method suffers from hysteresis due to the high energy barrier between the solid and liquid phases, the solid-liquid interface in the coexistence method creates a channel between the two phases, so they are free to exchange and the hysteresis is removed. These observations naturally suggest the possibility of combining these two methods.

Let us imagine the case of small size solid-liquid coexistence. We expect to gain a significant speed boost as the system size is significantly reduced. At the same time, we will certainly face another problem: the interface is not stable in small systems. In isothermal-isobaric (constant *NPT*) simulations, the system will quickly turn into a pure state, either solid or liquid, and never go back again to the coexisting state, during the short time scale (∼10 ps) we can reach.

Although it fails to maintain two stable phases, we find that small-size coexistence simulation contains plenty of

[a]qhong@caltech.edu

thermodynamic information. When two phases coexist at the beginning, the system evolves following thermodynamic rules, which govern the transition between the two phases and affect the probability distribution of the final pure states. By running many parallel small-size coexistence simulations and analyzing this probability distribution, we can obtain the relative stability of the two competing phases. In this article, we derive the theory that describes small-size coexistence simulation and demonstrate that it is a robust method for MP prediction.

Despite its similar name, our approach should be distinguished from the "two-phase thermodynamics" approach,[21–23] in which the liquid phase is represented as a fictitious mixture of a solid-like and hard-sphere-like free energy contributions.

The method is described in detail in Sec. II. We present the validation of the method and the study on its system-size dependence in Sec. III. Then we apply it to DFT calculations of melting temperatures. Discussions and conclusions can be found in Sec. IV.

II. METHODS

A schematic illustration of the idea is shown in Fig. 1. Solid-liquid coexisting systems are prepared by heating and melting half of the solid, while the other half is fixed frozen. Starting from a set of different coexistence configurations, isothermo-isobaric (*NPT*) MD simulations are carried out to trace the evolution. After several picoseconds, the two interfaces annihilate with each other and all simulations end with homogeneous phases, either solid or liquid.

We attempt to extract information regarding the MP from the ratio $N_{\text{liquid}}/N_{\text{solid}}$, where N_{liquid} and N_{solid} are, respectively, the numbers of simulations that terminate in a completely liquid or completely solid state starting from an initial

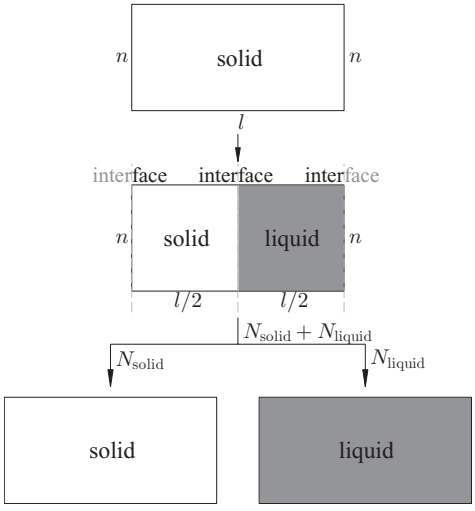

FIG. 1. Schematic illustration of how small-size coexistence method is executed in practice. Starting from $n \times n \times l$ supercell with atoms on their ideal solid positions, we heat and melt the right half to obtain solid-liquid coexistence configurations. Then many parallel *NPT* MD simulations (here a total of $N = N_{\text{solid}} + N_{\text{liquid}}$) are performed, in order to measure the probability distribution.

half-half solid-liquid coexistence. To calculate this ratio, we view the interface position x (defined by the atomic fraction of liquid phase) as obeying a random walk with a drift related to the free energy difference between the liquid and the solid phases. The initial state is $x = 0.5$ and we track the system until it reaches either $x = 0$ or $x = 1$, which are considered completely "absorbing" states, because the free energy of formation of the interface so large that, once it has disappeared, it would not reappear in a time frame reachable by our simulations. In between those two absorbing states, the free energy of system is given by $G(x) = G^s + G^{l-s}x$, with $G^{l-s} \equiv G^l - G^s$, and where G^l and G^s, respectively, denote the free energies of the whole system if it were entirely liquid or entirely solid. In a time step Δt, the system can jump from x to $x + \Delta x$ or to $x - \Delta x$ or stay in place at x. The system jumps with an attempt frequency ν (which can be assumed constant, without loss of generality, since the activation entropy can absorb any change in ν). When jumping from x to $x + \Delta x$, the system faces a free energy barrier $G_B + G^{l-s}\Delta x/2$, where G_B is a barrier measured relative to the average free energy of the initial and final states. The probability of jumping from x to $x + \Delta x$ in a time interval Δt is thus

$$p_{x\to x+\Delta x} = \nu \exp(-\beta(G_B + G^{l-s}\Delta x/2))\Delta t, \tag{1}$$

where $\beta = (k_B T)^{-1}$ and k_B is Boltzmann's constant. Similarly, the probability of jumping from x to $x - \Delta x$ is

$$p_{x\to x-\Delta x} = \nu \exp(-\beta(G_B - G^{l-s}\Delta x/2))\Delta t. \tag{2}$$

To avoid carrying through unnecessary quantities, it is convenient to work with jump probabilities conditional on a jump (by either $+\Delta x$ or $-\Delta x$) taking place, given by

$$\tilde{p}_{x\to x+\Delta x} \equiv \frac{p_{x\to x+\Delta x}}{p_{x\to x+\Delta x} + p_{x\to x-\Delta x}}, \tag{3}$$

$$\tilde{p}_{x\to x-\Delta x} \equiv \frac{p_{x\to x-\Delta x}}{p_{x\to x+\Delta x} + p_{x\to x-\Delta x}}. \tag{4}$$

As the system undergoes a random walk, the interface position goes through a sequence of values x_i. A useful observation is that for any sequence x_i converging to 1 there exists a corresponding sequence $\bar{x}_i \equiv 1 - x_i$ converging to 0. In general, the two sequences do not necessarily have the same probability. Indeed, the ratio of their probabilities can be derived as follows. Let r and l be the number of times x_i jumps towards $+\Delta x$ and towards $-\Delta x$, respectively. Note that

$$\begin{aligned}
&\frac{\prod_{i=1}^{l+r} \tilde{p}_{x_i\to x_{i+1}}}{\prod_{i=1}^{l+r} \tilde{p}_{\bar{x}_i\to \bar{x}_{i+1}}} \\
&= \prod_{i=1}^{l+r} \frac{\tilde{p}_{x_i\to x_{i+1}}}{\tilde{p}_{(1-x_i)\to(1-x_{i+1})}} = \prod_{i=1}^{l+r} \frac{p_{x_i\to x_{i+1}}}{p_{(1-x_i)\to(1-x_{i+1})}} \\
&= \frac{(\exp(-\beta G^{l-s}\Delta x/2))^r (\exp(\beta G^{l-s}\Delta x/2))^l}{(\exp(\beta G^{l-s}\Delta x/2))^r (\exp(-\beta G^{l-s}\Delta x/2))^l} \\
&= \exp(-\beta G^{l-s}\Delta x(r-l)) \\
&= \exp(-\beta G^{l-s}/2),
\end{aligned} \tag{5}$$

since if x_i goes from 1/2 to 1, then $\Delta x(r - l) = 1/2$. Now, if we consider every possible path x_i (of any length) going to 1,

the ratio of the total probabilities is

$$\begin{aligned}\frac{N_{\text{liquid}}}{N_{\text{solid}}} &= \frac{\sum_{\{x_i\}} \prod_i \tilde{p}_{x_i \to x_{i+1}}}{\sum_{\{x_i\}} \prod_i \tilde{p}_{(1-x_i)\to(1-x_{i+1})}} \\ &= \frac{\sum_{\{x_i\}} \exp(-\beta G^{l-s}/2) \prod_i \tilde{p}_{(1-x_i)\to(1-x_{i+1})}}{\sum_{\{x_i\}} \prod_i \tilde{p}_{(1-x_i)\to(1-x_{i+1})}} \\ &= \exp(-\beta G^{l-s}/2) \frac{\sum_{\{x_i\}} \prod_i \tilde{p}_{(1-x_i)\to(1-x_{i+1})}}{\sum_{\{x_i\}} \prod_i \tilde{p}_{(1-x_i)\to(1-x_{i+1})}} \\ &= \exp(-\beta G^{l-s}/2). \end{aligned} \tag{6}$$

The factor 1/2 in this Boltzmann-like expression arises because our probabilities are conditional on the system starting in specific state (half liquid, half solid) and ending in one of the two specific states (entirely liquid or solid). If the system were started in a randomly chosen state and were left to evolve indefinitely (repeatedly melting and solidifying at random), then the ratio of the probabilities of the simulation cell being all liquid and all solid would yield, asymptotically, the usual Boltzmann expression $\exp(-\beta G^{l-s})$, without the 1/2 factor.

Since G^{l-s} equals zero at MP, one could locate MP where N_{liquid} equals N_{solid}. However, it is not an efficient way to proceed because it usually takes several iterations to approach MP while all the trial calculations (away from the MP) are wasted. To avoid this, we propose the following fitting method which not only takes advantages of all available calculations, but also yields more melting properties in addition to the MP.

We compute the ratios $f(T) = N_{\text{liquid}}/(N_{\text{solid}} + N_{\text{liquid}})$ on a set of different temperatures. As T increases, G^{l-s} turns gradually from positive to negative, so f changes smoothly from 0 to 1. Thus, we can obtain MP through fitting the expression. In practice, in order to calculate more melting properties, we combine this relation with enthalpy, since it can be easily calculated as an average over an MD trajectory:

$$H(T) = H^s(T) + H^{l-s}(T) \frac{\exp[-\beta G^{l-s}(T)/2]}{1 + \exp[-\beta G^{l-s}(T)/2]}, \tag{7}$$

where

$$H^s(T) = H^s(T_m) + C_p^s (T - T_m), \tag{8}$$

$$H^{l-s}(T) = H^{l-s}(T_m) + C_p^{l-s} (T - T_m), \tag{9}$$

$$G^{l-s}(T) = \frac{T_m - T}{T_m} H^{l-s}(T_m) - C_p^{l-s} \frac{(T - T_m)^2}{T_m}. \tag{10}$$

We derive Eq. (10) in the Appendix. By fitting $H(T)$ to T, we obtain melting properties, e.g., melting temperature T_m, solid and liquid enthalpies $H^{s/l}(T_m)$ at T_m, and heat capacities $C_p^{s/l}$.

III. RESULTS

This section consists of two parts. In the first part, the method is extensively studied on empirical potentials. Although our method is primarily intended to be used with DFT calculations, empirical potentials enable us to extensively test and study our method, using an accurate benchmark (a large cell coexistence simulation). The validation of the method is first demonstrated. Then size effect is studied by gradually reducing the system size to around 100 atoms, which is suitable for DFT calculations. In the second part, we apply the method to DFT calculations to show that it provides an effective way to predict melting temperatures.

A. Empirical potentials

1. Validation

We test our method on a relatively large system (6 × 6 × 12 supercell containing 864 atoms) and a tantalum embedded atom method (EAM) potential.[24] The MP predicted is compared with the benchmarks, which we obtain by both large-size solid-liquid coexistence method and the free energy method. The excellent agreement demonstrates that our method is valid and it is capable to compute MP accurately.

To generate starting configurations ($x_{\text{liq}} = 0.5$) for MD simulations, we melt the right half of the bcc Ta lattice by heating it to a very high temperature (about 4 times the estimated MP), while the left half is fixed at its ideal bcc position. After the right half melts completely, we continue the MD simulation for several thousand steps and capture different coexisting configurations uniformly from the MD trajectory. Each snapshot, a half-and-half combination of freezed solid and superhot fluid, serves as a starting point for one MD simulation.

NPT MD simulations are carried out to trace the evolution of coexisting systems, as is commonly done (see, e.g., Ref. 10). Here, the thermostat is conducted under the Nose-Hoover chain formalism.[25–28] The barostat is realized by adjusting volume every 200 steps according to average pressure. (Although this does not formally generate an isobaric ensemble, we find it effective to change volume smoothly and to avoid the unphysical large oscillation caused by commonly used barostats.) During the first hundred femtoseconds, the temperature difference between the solid and the liquid is eliminated through fast heat transfer. The thermostat quickly turns the whole system to the designed temperatures, while the solid and liquid compositions are still approximately 0.5, as the time scale is too short for any phase transition to occur.

Each MD simulation undergoes either freezing or melting to a pure state. Methods including bond order parameter[29,30] and atomic displacements are used to distinguish between solid and liquid, and to determine whether a system has completely frozen or melted. We show in Fig. 2 the evolution of 50 independent MD trajectories at 3325 K, from which we can clearly see phase transitions, as they all end at either a higher (liquid) or lower (solid) enthalpy. The final enthalpy is collected from each trajectory, shown as green dots in Fig. 3. Enthalpies and heat capacities are fitted for the solid and the liquid state separately, according to Eqs. (8) and (9). At each temperature, the combined enthalpy of solid and liquid together and its standard error are computed based on binomial distribution, shown as blue bars. Finally, melting temperature is obtained through fitting the relation between enthalpy and temperature according to Eq. (10). As shown in

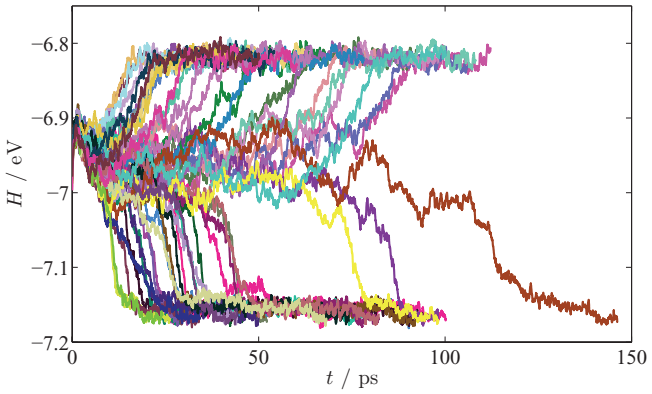

FIG. 2. Enthalpy H versus time t shows the evolution of 50 independent MD systems ($6 \times 6 \times 12$ supercell, 864 atoms) at 3325 K. It is clear that each trajectory ends finally in a pure state, either solid (lower enthalpy) or liquid (higher enthalpy).

both Table I and Fig. 3, the close agreement between the results and the benchmarks strongly suggests that our method is valid.

There is another interesting phenomenon we should note in Fig. 2. Although we have assumed that a simulation will never go back to coexistence only after it reaches a pure phase, this is not exactly true. Even when the fraction of a certain phase is nonzero but small enough, the two interfaces on its boundaries interact so strongly that they intend to annihilate with each other. According to Fig. 2, the ultimate fate of an MD simulation (fully liquid or fully solid) is only "undetermined" if its composition is within a certain region, e.g., between −7.0 and −6.9 in Fig. 2. As soon as it steps outside the region, i.e., the composition of one phase is large enough, this advantage is so large that it will never be overruled. This implies that the range $[x_{\min}, x_{\max}]$ of liquid fraction x where the system truly evolves as a random walk is smaller than [0, 1]. To account for this, we introduce one more parameter in to Eq. (6) when fitting to reflect the *a priori* unknown length $l_x = x_{\max} - x_{\min}$. It is straightforward that we can rewrite Eq. (6) as follows, provided that $[x_{\min}, x_{\max}]$ is symmetric,

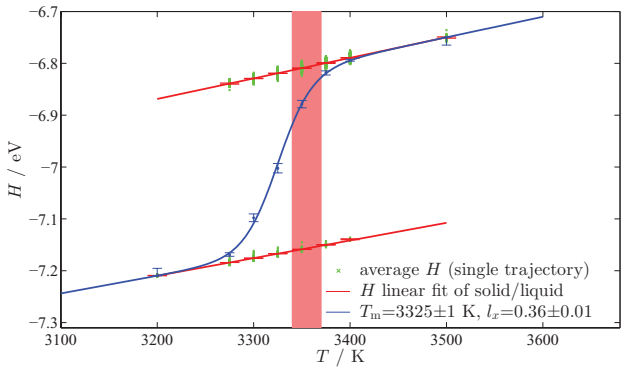

FIG. 3. The melting properties fitted according to Eqs. (7)–(10). The average enthalpies are shown in green dots. The solid and liquid parts (two red lines) are first fitted separately to obtain enthalpies and heat capacities, according to Eqs. (8) and (9). Then, we combine the two phases and fit to Eq. (10) to compute MP. The predicted MP agrees with the benchmarks (the pink vertical bin).

TABLE I. Melting properties and comparison with benchmarks.

	This method	Free energy method	Coexistence method
T_m (K)	3325	3370	3340
$H^{l-s}(T_m)$ (eV)	0.348	0.353	
C_p^s ($\times 10^{-4}$) (eV K^{-1})	3.49	3.24	
C_p^l ($\times 10^{-4}$) (eV K^{-1})	3.88	3.98	

i.e., $x_{\min} + x_{\max} = 1$:

$$\frac{N_{\text{liquid}}}{N_{\text{solid}}} = \exp\left(-\beta G^{l-s} l_x/2\right). \tag{11}$$

Observing that the interaction of two interfaces is determined dominantly by the distance d between them, we expect l_x to approach 1 asymptotically as we elongate the cell along the direction perpendicular to the interface, which renders d negligible compared the total length of the cell. We calculate the value of l_x for different length l in cell size $n \times n \times l$. When the length l increases, we find l_x approaches 1 as we expected, shown in Fig. 4. This predicted property serves as another proof on the validity of our theory.

We note that although our theory is perfect (i.e., T_m is exact and $l_x = 1$) only when the system size is large enough, the accurate calculation of melting temperature does not necessarily require such large size. Take the study in Fig. 4 as an example. T_m is calculated as 3325 and 3312 K for $l = 12$ and 32, respectively, though l_x is as different as 0.36 and 0.89. Melting temperature calculations are accurate even on small system sizes, as we will show in Sec. III A 2.

2. Size effect

After we demonstrate that our method is valid in the large system limit, we gradually reduce the system size down to around 100 atoms, a size suitable for DFT calculations. The size effect is studied systematically in this section. The three dimensional space is catalogued into two groups, i.e., the two

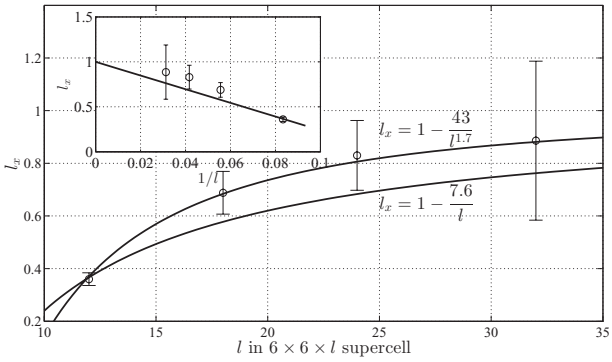

FIG. 4. l_x as a function of cell length l in supercell size $6 \times 6 \times l$. We calculate l_x on $l = 12$, 18, 24, and 32. The value of l_x approaches 1 asymptotically as l increases. Two curves, which are functions of l^{-1} and $l^{-1.7}$, respectively, are fitted to show the asymptote. Although a simple geometrical argument suggests an exponent of −1, we find that, in practice, the convergence is slightly faster, perhaps because of other size effects, such as the periodic image interactions, an additional higher-order effect that fades with system size. In the inserted small plot, the data points are fitted to a line $l_x = 1 - d/l$.

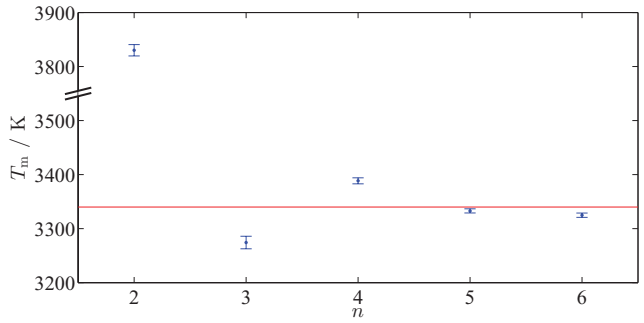

FIG. 5. Finite-size effect caused by system size n in $n \times n \times l$. Melting temperatures are calculated on $n \times n \times 12$ supercells with n ranging from 2 to 6, following the same scheme described in Sec. III A 1. We find that MP calculations are still correct for n down to 3.

dimensions in parallel to the interface and the last dimension perpendicular to the interface. The contributions of these two factors are treated separately. We find that the error of MP is still within 100 K even if the supercell size is reduced to $3 \times 3 \times 6$ (108 atoms), which is appropriate for DFT MD calculations.

We first study the directions parallel to the interface plane. As the box size becomes smaller in these two directions, the periodic constraints exert more impact on both phases, especially on the liquid, since the correlation length is truncated by the box vectors. Therefore, the calculated MP starts to deviate from the true value. We decrease supercell sizes ($n \times n \times 12$) from $n = 6$ down to 2, and calculate MP for each size, following the same recipe. The size dependence of MP is shown and compared in Fig. 5. We find that even for system size as small as $n = 3$, the finite size effect is still reasonably small.

We then study the size effect along the direction perpendicular to the interface. As we reduce the vector along this direction, the interaction among interfaces becomes stronger, either attracting or repelling each other and thus biasing the result. We gradually decrease l from 12 to 4. n is set to 3, because it is small enough and it still leads to the correct MP, according to the analysis in the previous paragraph. We find that the error is still small even for $3 \times 3 \times 6$, as shown in Fig. 6.

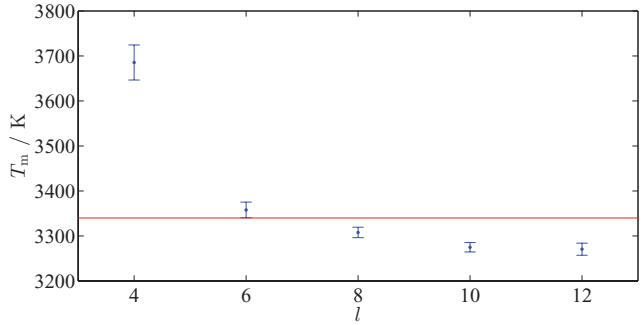

FIG. 6. Finite-size effect caused by system size l in $n \times n \times l$. Melting temperatures are calculated on $3 \times 3 \times l$ supercells with l from 12 down to 4. We find that melting temperature is still accurate even for system size as small as $3 \times 3 \times 6$.

3. More tests

Employing empirical potentials, we test the method on different materials, including bcc niobium,[31] fcc copper,[32] and ionic material sodium chloride.[33] For each material, we study the finite-size effect caused by system size $n \times n \times l$. The MPs calculated are presented in Fig. 7. For super-cells with $n : n : l = 1 : 1 : 2$ (so the box size is approximately $a \times a \times 2a$), we summarize the finite-size error in Fig. 8. When system size is large, the excellent agreement with the benchmarks serves as strong evidence of the reliability of our method. In order to achieve the accuracy within 100 K in MP calculation, we find that it is usually sufficient if the system size is larger than 10 Å and if it contains more than 100 atoms. This property strongly supports our claim that this method can be applied to DFT calculations.

B. DFT calculations

1. Tantalum at ambient pressure

As a simple example, we first apply our method to the MP calculation of Ta at ambient pressure.

The simulations are performed on a $3 \times 3 \times 6$ bcc supercell, containing 108 atoms. All electronic structures are calculated by the Vienna *Ab-initio* Simulation Package (VASP),[34–36] with the projector-augmented-wave (PAW)[37] implementation and the generalized gradient approximation (GGA) for exchange-correlation energy, in the form known as Perdew-Burke-Ernzerhof (PBE).[38] Both the valence 6*s*, 5*d*, and inner core 5*p* electrons (denoted as PBE-core) are included. The electronic temperature is accounted for by imposing Fermi distribution of the electrons on the energy level density of states (DOS), so it is consistent with the ionic temperature. The plane wave energy cutoff is set to 224 eV and it is further increased to 500 eV for pressure correction. A special k-point[5,8] (0.00 0.25 0.25) is used throughout the calculations. To estimate the error of using this single k-point, we compute its difference to fully converged value, on randomly chosen configurations including both solid and liquid. The root mean square error is less than 1 meV/atom.

As shown in Fig. 9 and Table II, the melting temperature calculated is 3200 K, only ~60 K lower than the experiment. This magnitude of error is consistent with our previous size-effect study in Sec. III A 2. It is interesting that, by contrast, the calculated heat of fusion and heat capacity (as shown in Table II) differ more significantly from experiment. These observations are not contradictory. First, finite size effects could introduce a similar bias in the free energies of both the solid and the liquid phases, so that such bias would manifest itself in phase-specific quantities but would only have a second-order effect on the melting point. Second, although the argument of error cancellation between phases is not applicable to the heat of fusion, another possible error cancellation mechanism is between entropy and enthalpy, as these two quantities tend to change in concert but affect the free energy in opposite ways. Periodic boundary conditions cause the long-range pair-correlation of the liquid to exhibit some solid-like character. This could lead to a larger reduction in

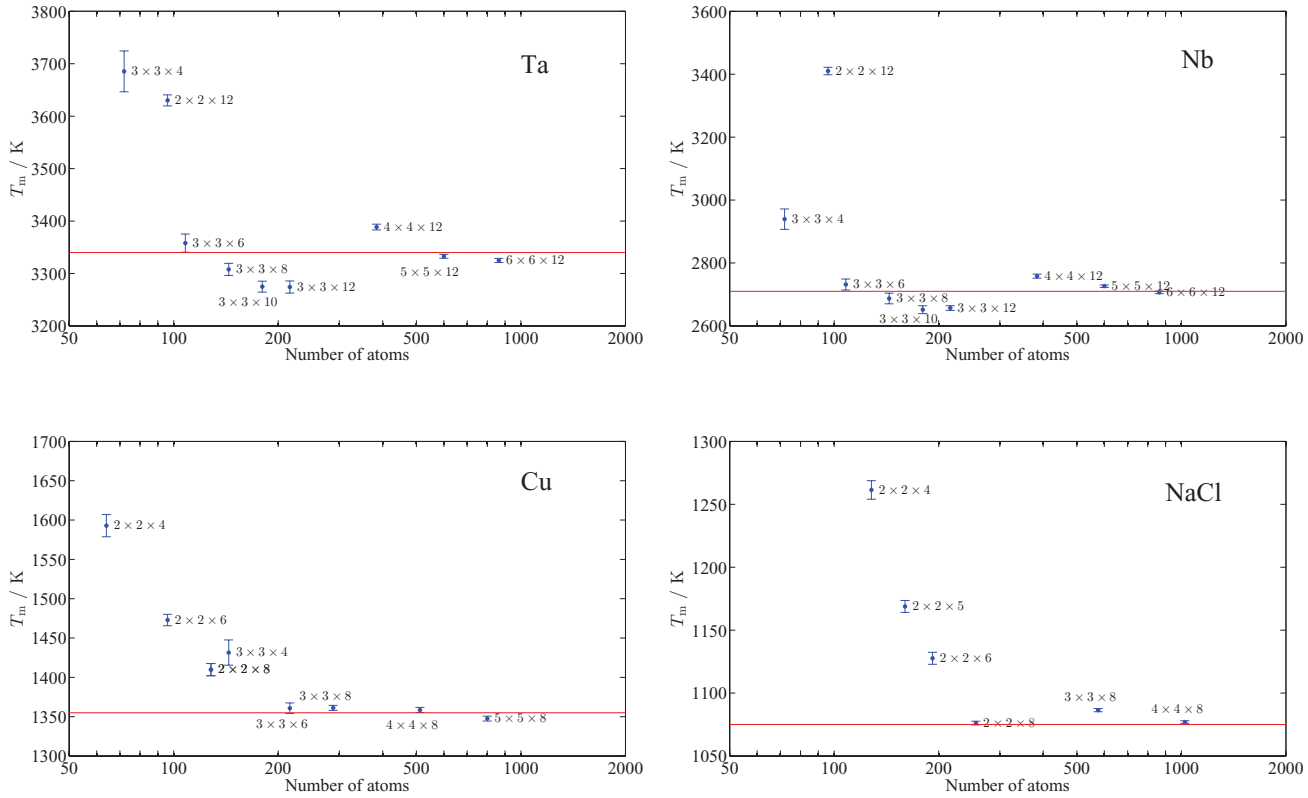

FIG. 7. Various tests on different materials to study the finite-size effect on melting temperature calculations. Tests are conducted on bcc tantalum, niobium, fcc copper, and ionic sodium chloride. These tests suggest that if we perform calculations with around 100–200 atoms, we are likely to achieve an accuracy of 100 K in melting temperature.

both the entropy and the enthalpy of the liquid phase, relative to the solid phase. Further study on finite-size effects would be useful to confirm this and could suggest approaches to include finite-size corrections to the current method.

We evaluate the importance of the core 5*p* electrons, by freezing them in electronic structure calculations (denoted as PBE-valence). As shown in Table III and Fig. 10, the new PBE valence-only pseudo-potential reduces the calculated MP and worsens the results. This necessity of 5*p* core electrons is consistent with previous findings.[39]

We also test the effect of exchange-correlation functionals by changing it to the Perdew-Wang 1991 (PW91) form[40] (denoted as PW91-core). As summarized in Table III and Fig. 10, it also reduces the calculated MP and worsens the results. This small discrepancy is not strange, since there have been evidences showing the differences between PBE and PW91, although they are regarded as almost identical GGA functionals most of the time. Our results indicate that PBE is a better exchange-correlation functional than PW91 in the case of tantalum melting.

The impact of PW91-core and PBE-valence can be quantified in the following way. At the MP, the free energy difference is zero, i.e.,

$$\Delta\mu = \mu_{\text{liquid}} - \mu_{\text{solid}} = 0, \tag{12}$$

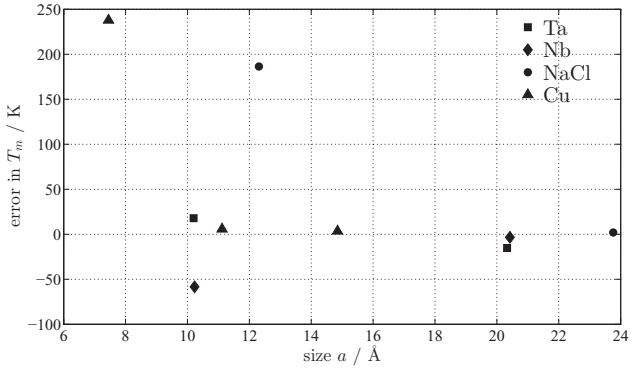

FIG. 8. The impact from box size $a \times a \times 2a$ on the error of MP calculation. When the size is larger than 10 Å, an accuracy of 100 K in T_m is usually guaranteed, though for ionic materials it is relatively less accurate probably due to the long-distance Coulomb interaction.

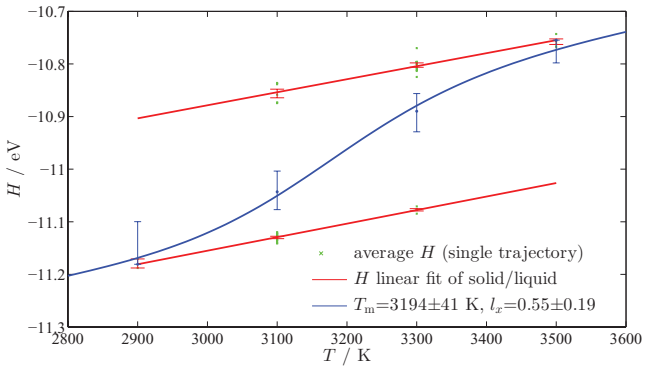

FIG. 9. The melting properties fitted according to Eqs. (7)–(10). All calculations are based on PBE-core pseudo-potential.

TABLE II. Melting properties and comparison with benchmarks.

	This method	Experiment
T_m (K)	3200	3258
$H^{l-s}(T_m)$ (eV)	0.274	0.379
C_p^s ($\times 10^{-4}$) (eV K^{-1})	2.57	4.34
C_p^l ($\times 10^{-4}$) (eV K^{-1})	2.52	4.57

TABLE III. Comparison of PBE-core, PW91-core, and PBE-valence.

	PBE Core	PBE Valence	PW91 Core	Experiment
T_m (K)	3200	2990	3070	3258
$\Delta\mu_\beta - \Delta\mu_\alpha$ ($\lambda = 0, 1$) (meV)	...	−2.5, −6.4	−6.8, −7.3	...

we employ the thermodynamic integration method to estimate the impact PW91-core and PBE-valence have on the free energy difference $\Delta\mu$:

$$\mu^\beta = \mu^\alpha + \frac{1}{N}\int_0^1 \langle H_\beta - H_\alpha\rangle_{H_\lambda} \mathrm{d}\lambda, \tag{13}$$

where β is PW91-core or PBE-valence, α is PBE-core and

$$H_\lambda = (1-\lambda)H_\alpha + \lambda H_\beta. \tag{14}$$

The integral is evaluated only at $\lambda = 0$ (PBE-core) and 1 (PW91-core or PBE-valence). Snapshots of pure solid and liquid are chosen randomly from MD trajectories of $\lambda = 0$ and 1, and the energy differences $H_\beta - H_\alpha$ are calculated on them. As summarized in Table III, PW91-core and PBE-valence stabilize liquid phase by 7 and 4 meV, respectively. Over-stabilized liquid results in a lower MP, thus qualitatively explains the MP trend predicted.

Similar to the procedure we have employed in Fig. 7, traditional coexistence method could serve as a benchmark to judge the quality of our calculation. However, such large-scale first-principles MD is computationally prohibitive. Here we perform such a check only on the relatively "less expensive" PBE-valence pseudo-potential. A $6 \times 6 \times 12$ supercell (864 atoms) containing solid and liquid coexistence is employed in NVE MD. As shown in Fig. 11, the MP is around 2900 K, in close agreement with the corresponding small-size coexistence calculation (2990 K), thus further confirming the reliability of our method.

2. bcc sodium under high pressure

A prototype simple metal at ambient conditions, sodium exhibits unexpected complexity under high pressure. One typical example is the so-called "reentrant" behavior, i.e., the melting curve of sodium reaches a maximum around 1000 K at ∼30 GPa followed by a pressure-induced drop, which extends to nearly room temperature at ∼120 GPa and over the stability regions of three solid phases.[41] There have been computational evidences supporting the experimental observation. Raty *et al.*[15] employed the fast-heating method and obtained a melting curve close to the experiments. Eshet *et al.*[42] used a neural-network potential based on DFT and calculated a melting curve through the free energy method. Despite of their successful capture of the reentrant behavior, the detailed melting points in these two articles are nevertheless quite different. The possible reason could be either the overheating problem in the former method, or the inaccuracy brought in by the neural-network method of the latter. Our small-size coexistence method provides an independent way to corroborate either one of these results.

Here we calculate the melting temperatures in the pressure range where the bcc structure is stable. The simulation techniques are similar as described in Secs. II–III B 1. We use a $3 \times 3 \times 6$ bcc supercell with 108 Na atoms. All calculations are performed by VASP with PAW and PBE. All 3*s* valence and 2*p* core electrons are included for electronic structure calculations, as the importance of the core 2*p* electrons is widely acknowledged.[42–44] Fermi distribution among the energy level density of states is imposed to realize the electronic temperature. The plane wave energy cutoff is set to 260 eV and it is further increased to 500 eV for pressure correction. A special k-point (0.00 0.25 0.25) is used throughout the calculations.

The calculated melting temperatures under various pressures are shown in Fig. 12 and Table IV. We successfully capture the reentrant point near (750 K, 40 GPa). Beyond this point, T_m starts to drop, and the specific volume change of melting, $\Delta V^{l-s} \propto \mathrm{d}T_\mathrm{m}/\mathrm{d}P$, turns from positive to negative, in agreement with the decrease of T_m. Our calculations agree

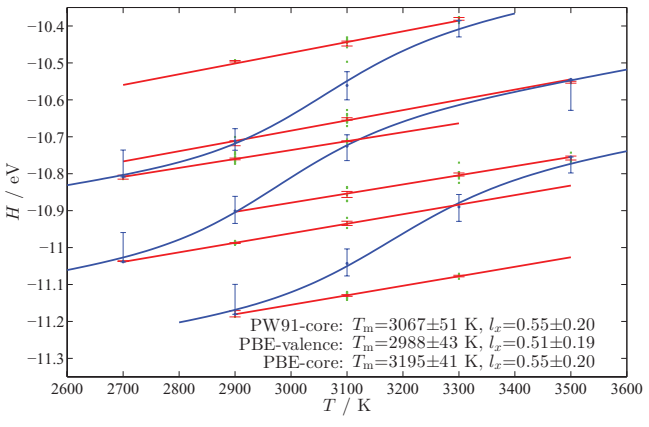

FIG. 10. Comparison of PBE-core, PBE-valence, and PW91-core, from bottom to top. The latter two are shifted vertically for clarity.

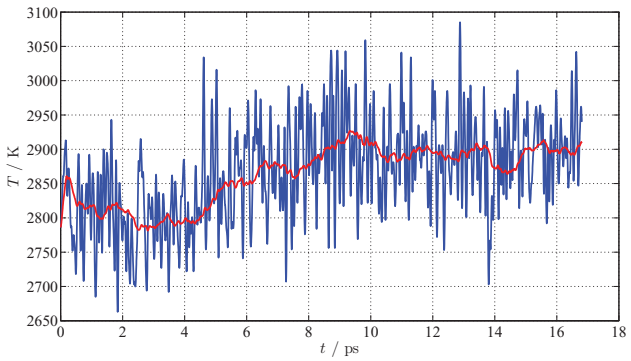

FIG. 11. *NVE* MD simulation of solid-liquid coexistence with 864 Ta atoms.

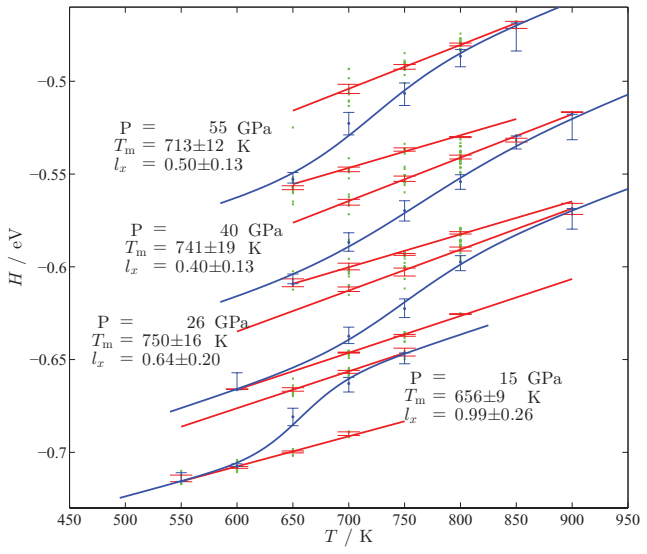

FIG. 12. The melting properties of Na up to 60 GPa fitted according to Eqs. (7)–(10).

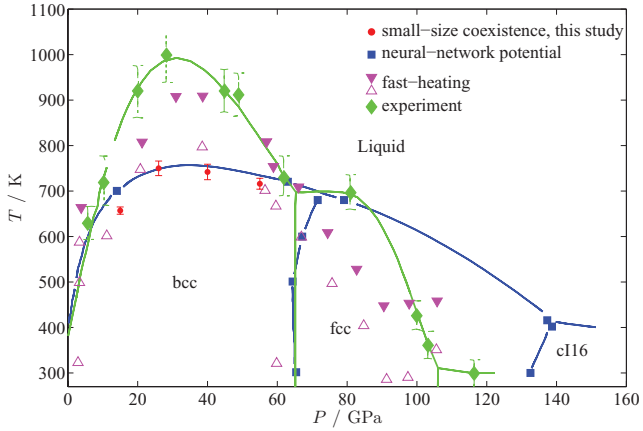

FIG. 13. Comparison of our results with other theoretical and experimental studies. Our melting temperatures at 20–50 GPa are presented as red dots. Green diamonds are experimental results from Ref. 41. Purple triangles are MPs by fast-heating method in Ref. 15. Blue squares are MPs by empirical potential in Ref. 42.

very well with the result reported in Ref. 42, while the MPs are still significantly lower than results from the fast heating method,[15] as summarized in Fig. 13. Our results suggest that the neutral network potential in Ref. 42 successfully mimics the interactions as comparable to DFT accuracy, while the over-heating issue, though relatively small, is still limiting the accuracy of the fast heating method employed in Ref. 15. To further verify our statement, we perform benchmarking through very expensive, large-size coexistence simulation (with 864 Na atoms). As Fig. 14 demonstrates, the melting temperature is around 750 K at 26 GPa, thus corroborating the reliability of our calculations. Although the MPs we compute, along with Ref. 42, are significantly lower than experiments, the good agreement with large-size coexistence calculations points to DFT errors, rather than a flaw of our method.

Our method's capability to obtain MP directly from DFT exhibits its potential to predict phase diagrams. Our melting curve in the bcc solid region, to the best of our knowledge, serves as the first directly first-principles and hysteresis-free computational evidence for the reentrant point of sodium.

3. NaCl at ambient pressure

After giving two examples on metals, we choose sodium chloride, an ionic material, as our last example. For a long time, MP calculations of ionic crystals were limited to only empirical potentials, probably due to the high expense for DFT correction by thermodynamic integration, as the corresponding high-quality empirical potentials are difficult to find. Recent development of computer power has made possible progresses on direct large-scale coexistence simulations of magnesium oxide[13] and lithium hydride.[14] However, these calculations are "extremely computationally intensive." Employing "Z-method," Belonoshko *et al.* have also successfully calculated MP for magnesium oxide.[17]

The simulation techniques are similar as Secs. II–III B 2. We use a 2 × 2 × 4 supercell containing 64 Na and 64 Cl atoms. Electronic structure calculations are performed by VASP PAW-PBE. Only valence electrons are included, i.e., the 3*s* electron for sodium and 3*s*, 3*p* electrons for chlorine. Electronic temperature is accounted for by a Fermi distribution. The energy cutoff is 280 eV and only Γ-point is used throughout the calculation. The error caused by using only Γ-point is less than 0.6 meV/atom.

As shown in Fig. 15, the MP is 1016 K, which agrees well with the experimental value, 1074 K.

TABLE IV. MP and volume change upon melting at different pressures.

P (GPa)	15	26	40	55
T_m (K)	657 ± 8	750 ± 16	742 ± 17	716 ± 12
ΔV^{l-s} (Å^3)	0.048	0.029	−0.005	−0.023

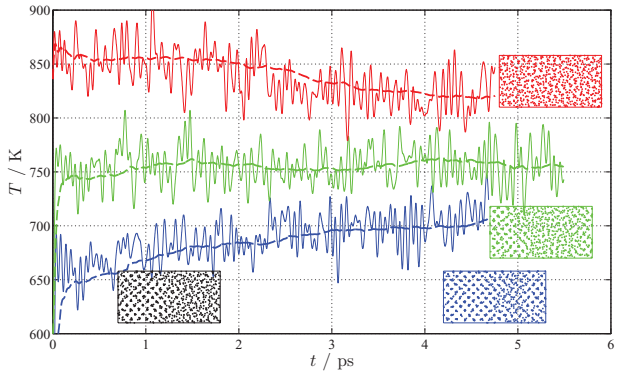

FIG. 14. Traditional large scale coexistence method (NVE) at different E. Systems with different E are shown in different colors. We plot in this figure the temperature evolution over time. Broken lines are time averages so they are more stable and clearer. Atomic configurations are included to help understand the results. Solid part has clear ordered patterns, while liquid part does not have. All starting from solid-liquid coexisting configurations (black), only system with proper E (green) remains in stabilized coexistence. A system with too high E will completely melt (red) and *vice versa* (blue). These tests suggest the melting temperature is around 750 K.

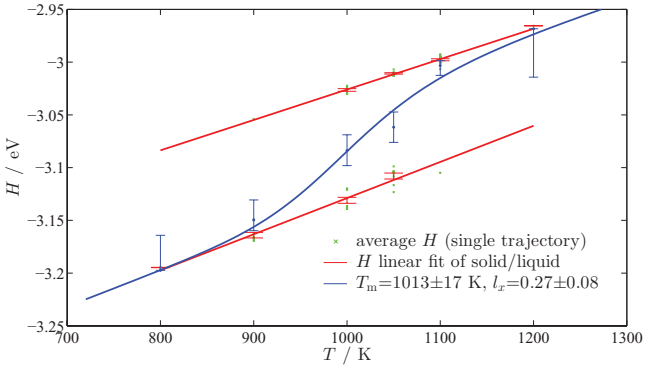

FIG. 15. The melting properties of NaCl fitted according to Eqs. (7)–(10).

IV. DISCUSSIONS AND CONCLUSIONS

The method we developed is based on formal theoretical grounds, derived in Sec. II, and its reliability is further strengthened by the excellent agreement with benchmarks, shown in Fig. 7, especially when system size is large. Various tests show that finite size effects are usually small and acceptable when the system size is larger than 10 Å and when it contains more than 100 atoms, a size manageable by DFT calculations. Our DFT examples demonstrate that our method is robust, efficient, and applicable for a wide class of materials.

To calculate a melting temperature, we usually need 30–60 MD simulations, each with an average length of 10–20 ps. Overall, our method saves significant computational costs compared to the traditional large-scale coexistence method. We list and compare in Table V the timings of several DFT examples we present in this article. In terms of total costs, our method is less expensive by approximately one order of magnitude. In addition, our method is inherently parallelizable, as we can run the whole set of MD simulations simultaneously. Therefore, it takes us the time of running only one single MD trajectory to finish a MP calculation, if we have plenty of computer resources. By contrast, one usually needs to perform, step by step, a long-time (usually more than 10 ps) MD simulation on a large-size system, in traditional coexistence method, which usually takes several months.

As discussed in Secs. III A 2 and III A 3, this method is subject to finite-size errors, i.e., about 100 K in MP for a system size of 100–200 atoms. Although this seems to be a major disadvantage of our method compared to others, we note that finite-size effect is a universal problem persisting in almost all MP prediction methods. (The large coexistence method is an exception. But it is nearly infeasible due to its high cost.) For example, fast-heating method and Z-method usually use comparable system size, so they suffer from similar size effect as well, in addition to the hysteresis problem. As another example, let us consider the free energy method based on empirical reference potentials followed by DFT corrections. One might argue that the finite-size error can be completely eliminated if convergence is achieved on empirical potentials with respect to system size. But this is not exactly true. As DFT corrections are usually performed on small-size systems, the final free energy calculated by this method is, strictly speaking, a DFT free energy on a small system plus a finite-size correction by the empirical potential. One can never guarantee that the finite size effect from an empirical potential will be the same (or even similar) to that of DFT. Therefore, the free energy method is also subject to finite-size errors.

TABLE V. Computational costs of our method and traditional coexistence approach. (Unit: $\times 10^3$ cpu hours on the Stampede cluster at TACC.)

	Traditional coexistence		Our method
	Single trajectory	Total	Total
Ta, PBE-valence	150[a]	∼500	30[b]
Na, $P = 26$ GPa	42, 48, and 35[c]	125	26[d]

[a]Shown in Fig. 11.
[b]Shown in Fig. 10 and Table III.
[c]Shown in Fig. 14, colored in blue, green, and red, respectively.
[d]Shown in Fig. 12 and Table IV.

We can approximately correct the finite-size errors by extrapolating the convergence behavior of both phases. The quasi-harmonic approximation provides a quick approach to estimate the correction in the solid phase, while radial distribution function[45] gives insight to the entropy of the liquid phase. The authors are currently working on this topic. Preliminary study shows promising results and sheds light on the improvement of the current method, making it more accurate and efficient, as we can further reduce the system size.

Another problem of finite size effect is that the system could be stabilized in a wrong phase, for either solid or liquid. This problem occurs when there is a competing alternative near the desired phase in the phase diagram. In reality, this competing phase is relatively less stable, but the finite-size effect could revert the stability relation of them, so that the simulation ends in a wrong structure. Therefore, we recommend that one should check the final structure of a MD trajectory to make sure that it is in the desired solid or liquid phase.

Although the method is robust in MP prediction, it also inherits the disadvantage of MD simulations, unfortunately. For example, it suffers from the well-known rare event problem. This renders it incapable for the following circumstances:

1. If the crystal structure of the solid is complex, the liquid half may fail to find the right crystal structure when solidifying, and it may form defected solid structures. Fortunately, this possibility is readily detectable in the simulations.
2. If there are more than one solid configurations and the stability is based on certain distribution in phase space, e.g., for some alloys, MD will fail to explore all configurations in limited computer time and find kinetically favored metastable structure.
3. If the elemental concentrations of the solid and the liquid are different at the equilibrium, MD is not capable to redistribute different atoms in each phase sufficiently fast. In systems where this occurs, the method can still be used to find melting points at compositions where congruent melting occurs. Free energy integration (on fairly small simulation cells) can be used to find the

solidus and liquidus at other compositions, using congruent melting points as free energy references.

However, we note here that these problems are also common to other methods, e.g., in the traditional large scale coexistence method.

It is interesting to compare our approach to the two-phase thermodynamics method, which calculates the entropies and free energies of liquids by partitioning the DOS into two parts, i.e., the solid-like Debye-model DOS and the gas-like hard-sphere DOS. This approach has been successfully applied to a wide variety of substances, including water[23] and many organic compounds.[22] Indeed, this method is surprisingly fast, since it only requires a MD simulation of ∼20 ps. However, the methods should be compared, not only in terms of computational costs, but also in terms of accuracy and their ability to converge to the correct answer as computational effort is increased. The two-phase thermodynamics approach relies on the assumption that the partitioning of DOS into two phases is always valid, which is not necessarily true. In addition, the harmonic approximation used for entropy calculations would be problematic at high temperatures, when anharmonic effects become significant. Due to these approximations, the two-phase thermodynamics method tends to underestimate the excess entropy by 5%.[23] Although small, this error is detrimental to melting temperature calculations. For instance, we estimate the error to be 40–60 meV in free energy and ∼500 K in melting temperature if the two-phase thermodynamics method is applied to the case of liquid-state copper, which we have studied extensively and achieved an accuracy of 100 K in melting temperature by DFT and particle insertion method.[8] Therefore, we conclude that our approach nicely fills the gap between the two phase thermodynamics method (at one extreme of the accuracy/cost trade-off) and methods based on large-scale coexistence (at the other extreme of the accuracy/cost trade-off). Our small-cell coexistence approach is immune to such problems. Its uncertainties only arise from finite size effects and statistical sampling, both of which can be systematically reduced by increasing computational resources. By contrast, the two-phase thermodynamic approach is not systematically improvable, because the partitioning and harmonic approximations are central to its convenient implementation.

To summarize, we have proposed an efficient and accurate method to calculate the MP of materials. This method is based on the statistical analysis of small-size coexistence MD simulations, so it circumvents both the hysteresis overheating problem in small system size and the prohibitive computer cost in traditional coexistence method. Using empirical potentials, we present the validation of the method and systematically study the finite-size effect on the MPs calculated. Through the DFT examples, we demonstrate the capability and flexibility of the method in its practical applications.

ACKNOWLEDGMENTS

This research was supported by ONR under Grant No. N00014-12-1-0196, and by NSF through XSEDE resources provided by NCSA, SDSC, and TACC.

APPENDIX: DERIVATION OF $\Delta_{s-l}G(T)$ AND $H(T)$

Assuming heat capacities $C_p^{s/l}$ are constants in the vicinity of MP. Then enthalpy and entropy are

$$H^{s/l}(T) = H^{s/l}(T_m) + C_p^{s/l}(T - T_m), \tag{A1}$$

$$S^{s/l}(T) = S^{s/l}(T_m) + C_p^{s/l} \ln \frac{T}{T_m}, \tag{A2}$$

where T_m is the melting temperature.

The Gibbs free energy difference $G^{l-s}(T)$ is

$$\begin{aligned} G^{l-s}(T) &= G^l(T) - G^s(T) \\ &= H^{l-s}(T) - TS^{l-s}(T) \\ &= H^{l-s}(T_m) + C_p^{l-s}(T - T_m) \\ &\quad - TS^{l-s}(T_m) - TC_p^{l-s} \ln \frac{T}{T_m} \\ &= (T_m - T)S^{l-s}(T_m) + C_p^{l-s}\left[T - T_m - T \ln \frac{T}{T_m}\right] \\ &= (T_m - T)S^{l-s}(T_m) - C_p^{l-s}\frac{(T - T_m)^2}{T_m} \\ &= \frac{(T_m - T)}{T_m}H^{l-s}(T_m) - C_p^{l-s}\frac{(T - T_m)^2}{T_m}. \end{aligned} \tag{A3}$$

[1] P. Hohenberg and W. Kohn, Phys. Rev. **136**, B864 (1964).
[2] W. Kohn and L. J. Sham, Phys. Rev. **140**, A1133 (1965).
[3] R. Jones and O. Gunnarsson, Rev. Mod. Phys. **61**, 689 (1989).
[4] O. Sugino and R. Car, Phys. Rev. Lett. **74**, 1823 (1995).
[5] G. de Wijs, G. Kresse, and M. Gillan, Phys. Rev. B **57**, 8223 (1998).
[6] D. Alfè, M. Gillan, and G. Price, Nature (London) **401**, 462 (1999).
[7] D. Alfè, G. Price, and M. Gillan, Phys. Rev. B **65**, 165118 (2002).
[8] Q.-J. Hong and A. van de Walle, J. Chem. Phys. **137**, 094114 (2012).
[9] V. Weber and D. Asthagiri, J. Chem. Phys. **133**, 141101 (2010).
[10] J. Mei and J. W. Davenport, Phys. Rev. B **46**, 21 (1992).
[11] J. Morris, C. Wang, K. Ho, and C. Chan, Phys. Rev. B **49**, 3109 (1994).
[12] A. B. Belonoshko, Geochim. Cosmochim. Acta **58**, 4039 (1994).
[13] D. Alfe, Phys. Rev. Lett. **94**, 235701 (2005).
[14] T. Ogitsu, E. Schwegler, F. Gygi, and G. Galli, Phys. Rev. Lett. **91**, 175502 (2003).
[15] J.-Y. Raty, E. Schwegler, and S. A. Bonev, Nature (London) **449**, 448 (2007).
[16] A. B. Belonoshko, N. V. Skorodumova, A. Rosengren, and B. Johansson, Phys. Rev. B **73**, 012201 (2006).
[17] A. B. Belonoshko, S. Arapan, R. Martonak, and A. Rosengren, Phys. Rev. B **81**, 054110 (2010).
[18] A. B. Belonoshko and A. Rosengren, Phys. Rev. B **85**, 174104 (2012).
[19] D. Alfe, C. Cazorla, and M. J. Gillan, J. Chem. Phys. **135**, 024102 (2011).
[20] A. B. Belonoshko, T. Lukinov, L. Burakovsky, D. L. Preston, and A. Rosengren, Eur. Phys. J. Spec. Top. **216**, 199 (2013).
[21] S. T. Lin, M. Blanco, and W. A. Goddard, J. Chem. Phys. **119**, 11792 (2003).
[22] T. A. Pascal, S. T. Lin, and W. A. Goddard, Phys. Chem. Chem. Phys. **13**, 169 (2011).
[23] C. Zhang, L. Spanu, and G. Galli, J. Phys. Chem. B **115**, 14190 (2011).
[24] Y. H. Li, D. J. Siegel, J. B. Adams, and X. Y. Liu, Phys. Rev. B **67**, 125101 (2003).
[25] S. Nosé, Mol. Phys. **52**, 255 (1984).
[26] S. Nosé, J. Chem. Phys. **81**, 511 (1984).
[27] W. G. Hoover, Phys. Rev. A **31**, 1695 (1985).
[28] G. J. Martyna, M. L. Klein, and M. Tuckerman, J. Chem. Phys. **97**, 2635 (1992).
[29] P. J. Steinhardt, D. R. Nelson, and M. Ronchetti, Phys. Rev. B **28**, 784 (1983).

[30]Y. T. Wang, S. Teitel, and C. Dellago, J. Chem. Phys. **122**, 214722 (2005).
[31]M. R. Fellinger, H. Park, and J. W. Wilkins, Phys. Rev. B **81**, 144119 (2010).
[32]M. I. Mendelev, M. J. Kramer, C. A. Becker, and M. Asta, Philos. Mag. **88**, 1723 (2008).
[33]J. Anwar, D. Frenkel, and M. G. Noro, J. Chem. Phys. **118**, 728 (2003).
[34]G. Kresse and J. Furthmüller, Comput. Mater. Sci. **6**, 15 (1996).
[35]G. Kresse and J. Furthmüller, Phys. Rev. B **54**, 11169 (1996).
[36]G. Kresse and D. Joubert, Phys. Rev. B **59**, 1758 (1999).
[37]P. Blöchl, Phys. Rev. B **50**, 17953 (1994).
[38]J. Perdew, K. Burke, and M. Ernzerhof, Phys. Rev. Lett. **77**, 3865 (1996).
[39]S. Taioli, C. Cazorla, M. J. Gillan, and D. Alfe, Phys. Rev. B **75**, 214103 (2007).
[40]Y. Wang and J. P. Perdew, Phys. Rev. B **44**, 13298 (1991).
[41]E. Gregoryanz, O. Degtyareva, M. Somayazulu, R. J. Hemley, and H. K. Mao, Phys. Rev. Lett. **94**, 185502 (2005).
[42]H. Eshet, R. Z. Khaliullin, T. D. Kuhne, J. Behler, and M. Parrinello, Phys. Rev. Lett. **108**, 115701 (2012).
[43]E. R. Hernandez and J. Iniguez, Phys. Rev. Lett. **98**, 055501 (2007).
[44]A. Yamane, F. Shimojo, and K. Hoshino, J. Phys. Soc. Jpn. **77**, 064603 (2008).
[45]B. B. Laird and A. D. J. Haymet, Phys. Rev. A **45**, 5680 (1992).